Hydro-mechanical response of crushed argillite and bentonite mixtures as sealing material

Jean-Claude Robinet, Danai Tyri, Irini Djeran-Maigre

Our reference: ENGEO 106140
Article reference: ENGEO_ENGEO_2020_1180
Article title: Hydro-mechanical response of crushed argillite and bentonite mixtures as sealing material

AUTHOR LIST

Jean-Claude Robinet
Euro-Géomat Consulting, 45100, Orléans, France
email: robinet-jc@wanadoo.fr

Danai Tyri
Euro-Géomat Consulting, 45100, Orléans, France
Andra, Meuse/Haute-Marne Underground Research Laboratory, 55290, Bure, France
Univ Lyon, INSA Lyon, 69621, Villeurbanne, France
email: danai-panagiota.tyri@insa-lyon.fr

Irini Djeran-Maigre
Univ Lyon, INSA Lyon, 69621, Villeurbanne, France
email: irini.djeran-maigre@insa-lyon.fr

Alternatively, the author list could be appeared as bellow:
Research paper
Hydro-mechanical response of crushed argillite and bentonite mixtures as sealing material
Jean-Claude Robinet[a], Danai Tyri[a,b,c], Irini Djeran-Maigre[c]
[a] Euro-Géomat Consulting, 45100, Orléans, France
[b] Andra, Meuse/Haute-Marne Underground Research Laboratory, 55290, Bure, France
[c] Univ Lyon, INSA Lyon, 69621, Villeurbanne, France

CONTACT DETAILS:

Dr. Danai Tyri
Andra, Meuse/Haute-Marne Underground Research Laboratory, 55290, Bure, France
Phone: +33 6 85 51 66 92
Fax: not available
E-mail: danai-panagiota.tyri@insa-lyon.fr;danaityri@gmail.com

Hydro-mechanical response of crushed argillite and bentonite mixtures as sealing material

Abstract

Mixture of excavated Callovo-Oxfordian (COx) argillite and MX80 bentonite has been proposed as potential sealing material for the French deep geological disposal facility of radioactive waste. The mixtures hydro-mechanical behaviour was studied in order to assess their response on design requirements. At the as-compacted state, soil fabric analysed by the MIP technique, showed single-modal pore distribution for pure COx and bimodal pore distribution for samples containing MX80. All tested mixtures developed homogeneous behavior during compaction with no effect of MX80 presence. Swelling potential was evaluated by hydration tests under 4 MPa on highly compacted material (2.0 Mg/m^3). Swelling increase and saturated permeability reduction was obtained on bentonite content increment. Combining results of the present experimental work and remarks of previous researchers, the characteristic saturation potential slope was determined and exploited to estimate the swelling under 1, 4 and 7 MPa for various COx/MX80 mixtures compacted at different pressures. The experimental verification of the adopted method suggested an approach of identifying possible combinations in terms of compaction and bentonite content that can fulfill design requirements.

Keywords: Callovo-Oxfordian argillite; MX80 bentonite; swelling potential; compressibility; pore distribution; OCR

Highlights

- Mixtures compressibility at initial water content is governed by COx argillite
- Bentonite presence results in bimodal pore size distribution
- Saturation potential slope estimates swelling under varied stresses for OC samples

1. Introduction

Engineering barriers located in natural deep geological formations are considered as suitable solution for the disposal of high-level waste (HLW) and intermediate-level long-lived radioactive waste (ILW-LL) (Andra, 2005a). Clay or crystalline formations are worldwide investigated as possible host rock for the waste disposal, due to many beneficial characteristics (e.g. high mechanical stability, low hydraulic conductivity, self-sealing potential, capacity for retardation of radionuclides transport). The disposal facilities indicate the construction of a complex network of drifts and shafts. The waste packages are placed on specifically designed containers and then installed inside tunnels. The excavation damaged zone (EDZ) created during the drift construction generates possible flow paths and potential transport of nuclides (Imbert and Villar, 2006; Armand et al., 2014). On the other hand, groundwater that gradually infiltrates the underground repository will cause the degradation of the waste container, having a negative impact on the waste confinement. Therefore, sealing materials in varied forms (blocks/pellets/in situ compacted material) are planned to be installed in key-positions of the structure, to minimize water circulation. In parallel, the remaining openings will be backfilled to limit the propagation of the EDZ, maintaining the properties of the sealing zone (Andra, 2013, 2005b; Foin et al., 2015).

In this context, the use of expansive clays is proposed, due to the high swelling capacity and low permeability developed on hydration (Komine, 2004a; Molinero Guerra et al., 2018; Pusch, 1982; Villar et al., 2012; Wang et al., 2012). The swelling clay will absorb water and expand, filling up voids inside the emplaced material as well as voids between the gallery and the EDZ, ensuring the waste confinement. Nonetheless, the swelling developed upon the infiltration must be adequate to achieve this sealing without risking the stability of the structure.

In France, Andra (National Radioactive Waste Management Agency) has chosen the Callovo-Oxfordian (COx) argillaceous formation as host rock for the disposal of the HLW and ILW, approximately 500 m below the surface. The repository construction involves the gallery excavation of tens of kilometres,

which produces a significant quantity of excavated COx. The reuse of the excavated COx as sealing and/or backfill material is examined for the underground repository, presenting great environmental and economic advantages (Tang et al., 2011a; Wang et al., 2012). One of the suggested techniques considers the sealing material implementation in prefabricated blocks. According to design requirements, the developed swelling upon hydration should fill initial voids estimated approximately at 10% (i.e. voids between the blocks, between the blocks and the gallery walls and notable voids induced by the lining removal), while stresses range between 1 to 7 MPa are applied (Chandler et al., 2002). Additionally, the intrinsic permeability upon the materials saturation (i.e. when degradation of waste container occurs) needs to be low enough to prevent water circulation on the repository ($<10^{-18}$ m^2) and radionuclide transfer.

In that framework, the behaviour of expansive clays such as bentonite-based materials has been widely examined over the years in terms of swelling capacity (Komine and Ogata, 1999; Villar and Lloret, 2008; Seiphoori et al., 2014; Barast et al., 2017) and hydraulic conductivity (Komine, 2004b; Hoffmann et al., 2007; Manca, 2015). Both properties are strongly affected by factors related to material micro and macro-structure. Depending on the volume conditions during hydration, the swelling capacity is expressed by (i) the swelling pressure which is developed on constant volume conditions and (ii) the swelling potential, which is the strain allowed to be developed for given stress conditions (Sridharan et al., 1986; Feng et al., 1998; Rao, 2006; Zhang and Kröhn, 2019).

Soil's swelling behaviour is primarily related to the water molecules interaction with the clay mineral. Therefore, mineralogy (e.g. montmorillonite content) is the first key parameter for the swelling capacity. Porewater chemistry affects notably the swelling performance. On several studies, salt presence in the porewater has been reported as suppressing factor of swelling (Di Maio et al., 2004; Mishra et al., 2009; Lee et al., 2012; Chen et al., 2018, 2016;). Porewater's pH might be altered due to the design concept (i.e. alkaline pertubation because of extensive use of cement). Swelling reduction has been observed at high alkaline conditions, revealing the importance of structure conditions on the sealing/backfill performance

(Cuisinier et al., 2014; Karnland et al., 2007; Robinet et al., 2003; Ye et al., 2014). However, it has been established that the increase of material's dry density, can increase exponentially the developed swelling pressure (Pusch, 1982; Karnland et al., 2008; Seiphoori et al., 2014; Yigzaw et al., 2016), counterbalancing the negative environmental effects. In fact, decreased initial voids lead to water absorption directly by the interlayer network (Villar et al., 2012).

In the present study, a series of tests were conducted on COx argillite/MX80 bentonite mixtures to evaluate their hydro-mechanical response as sealing material. Highly compacted samples with initial dry density ρ_d of 2.0 Mg/m^3 were considered, in accordance with the densities of prefabricated blocks as sealing option. Mixtures compressibility and pore size distribution at the compacted state were studied, after performing oedometric tests at the material's initial water content conditions. The swelling potential and saturated permeability were examined by conducting swelling potential tests under 4 MPa using demineralized water. Based on previous observations, a method was adopted to determine the saturation potential slope for each COx/MX80 mixture. Subsequently, the mixtures' swelling potential profile was created, for materials compacted at higher stresses and hydrated under the investigated stress range (1-7 MPa), in order to identifying conditions that respect the design requirements.

2. Background

Material's initial density was identified as one of the parameters governing the swelling response. Density state is linked to the soil's stress history and over-consolidation ratio (OCR) can be used as indicator of this stress history. OCR is defined as the ratio of the maximum past consolidation effective stress to the present effective stress (Mitchell and Soga, 2005). However, on remoulded soil materials, the maximum consolidation effective stress corresponds to the maximum vertical stress applied upon the sample's loading path ($\sigma'_{i\,loading}$), while the present effective stress refers to the stress applied on the unloaded sample ($\sigma'_{i\,unloading}$).

Experimental studies on remoulded expansive clays showed that on the overconsolidated stress state, samples present clear swelling when hydrated under a constant vertical stress (Broc et al., 1988; Dang, 2007). More precisely, Dang (2007) performed oedometric paths for overconsolidated stress states, on partially saturated MX80 samples unloaded on different vertical stresses $\sigma'_{i\,unloading}$ (i.e. resulting in different OCR > 1). It was observed that all samples exhibited swelling on saturation, which increased with OCR increase (Figure 1). Nonetheless, the swelling on saturation for the samples compacted at the same $\sigma'_{i\,loading}$ with different OCR (due to different $\sigma'_{i\,unloading}$) form a common curve in the $e - log\sigma'_v$ plane, which is hereafter called "saturation potential curve", with λ_s the saturation potential slope. Based on these observations, an approach is adopted in the following sections to determiner the saturation potential slope of different COx/MX80 mixtures.

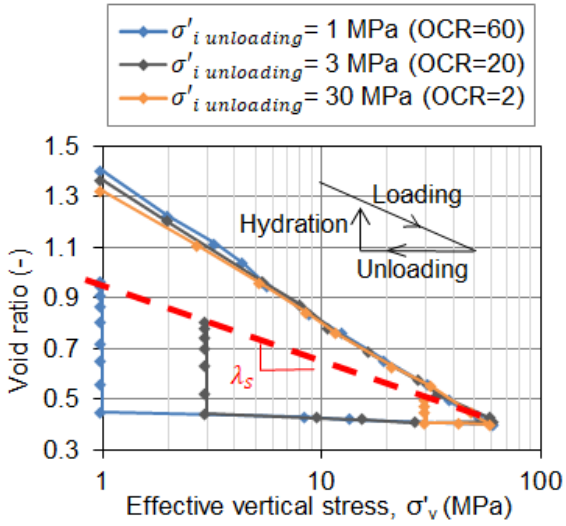

Figure 1 Variation of void ratio with applied vertical stress for overconsolidated MX80 samples, saturated under constant unloading vertical stresses. λ_s expresses the saturation potential slope (after Dang, 2007).

3. Materials and methods

3.1 Properties and fabric evolution of tested materials

An experimental study was conducted on mixtures composed of crushed COx excavated from Andra's URL and commercial MX80 bentonite, in various proportions of mass. At the -490 m, COx argillite

exhibits a rather homogeneous composition of tectosilicates (20%), carbonates (20–25%) and clay minerals (50–55%) together with subordinate pyrite and iron oxides (3%) (Armand et al., 2013). Tectosilicates are mainly quartz mineral, whereas carbonates are composed by calcite (Yven et al., 2007). The excavated COx used in this study was dried and crushed with initial water content of 3.9%. A fine product with maximum grain size of 300 μm was chosen, because it exhibited higher swelling response (Tang et al., 2011b). Commercial MX80 bentonite was used as additive to improve COx's swelling properties. MX80 is a sodium bentonite from Wyoming (USA) containing 80% smectites, 20% of other non-clay minerals (pyrite, albite anorthite quartz, muscovite) (Molinero Guerra et al., 2017). MX80 bentonite was also sieved at 300 μm.

Figure 2 presents the grain size distribution of the two materials resulted from the dry sieving method. The fine content (grains <80 μm) of COx is higher (F_c=40%) than MX80 bentonite (F_c=13%). Table 1 summarizes the physical and chemical properties of the materials, determined by using demineralized water. French Standards were used for the determination of liquid limit, plastic limit and MBV value (Methylene blue adsorption capacity) (AFNOR, 1993, 1995, 1998). Specific Surface Area (SSA) was estimated from MBV (Unikowski, 1982). The free swelling index (FSI) was measured following the AFNOR (2002) for the determination of the swelling capacity of bentonitic geosynthetics. According to the procedure, 2 g of dried powdered clay (< 160 μm) are progressively poured into a graduated cylinder, containing 100 cm^3 of demineralized water. The volume of swollen clay is measured after 24 h in units of cm^3/2g. The obtained values are in accordance with other studies for sodium bentonites (Barast et al., 2017; Davies et al., 2017).

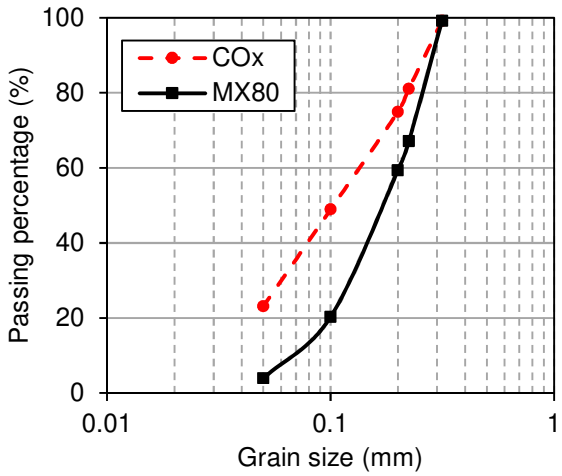

Figure 2 Grain size distribution of studied soils.

Table 1 Physical and chemical characteristics of the studied material.

Material	w (%)	LL (%)	PL (%)	MBV (g/100g)	SSA (m^2/g)	FSI (cm^3/2g)
COx	3.9	47	21	3.3	70	3.6
MX80	10.4	465	57	25	523	30

w: water content
PL: Plastic Limit obtained from Atterberg limits
LL: Liquid Limit obtained from Atterberg limits
MBV: Methylene Blue adsorption capacity Value
SSA: Specific Surface Area
FSI: Free Swelling Index

Studies on microstructure are used to further evaluate the hydro-mechanical behaviour of soils (e.g. swelling response, permeability, water retention properties). Fabric observations have shown a multi-scale pore network inside the material and revealed a double level in the structure, constituted by the macro and micropores (Gens and Alonso, 1992; Lloret et al., 2003; Romero, 2013). The first case is referring to voids existing between the aggregates (inter-aggregate) of the clay particles whereas the latter to the smaller voids inside the clay aggregate (intra-aggregate). Figure 3 presents the results of Mercury Intrusion Porosimetry (MIP) tests, which were carried out by using the Micromeritics AutoPore III 9420 porosimeter (maximum applied pressure 414 MPa), to study the pore size distribution (PSD) of the tested materials in the as-compacted state. COx and MX80 were compacted at their initial water content (3.9% and 10.4 % respectively), obtaining a dry density of 2.1 Mg/m^3. COx argillite presents a single modal PSD, with an inter-aggregate pore population to be recognised at 300 nm (macropores). Similar findings

were reported by Tang et al. (2011b) for a slightly lower dry density (2.0 Mg/m^3). On the other hand, a characteristic bimodal PSD is observed on pure MX80 bentonite (Hoffmann et al., 2007; Seiphoori et al., 2014; Molinero-Guerra et al., 2019). With the boundary identified around 0.1 µm, two groups of pores are recognized at 1.5 µm and 20 nm, referring to macro and micro-porosity respectively (Figure 3a). Even though the volume of macropores observed on COx is larger than the MX80 sample, COx's pore size is smaller. Therefore COx presents lower porosity (Figure 3b).

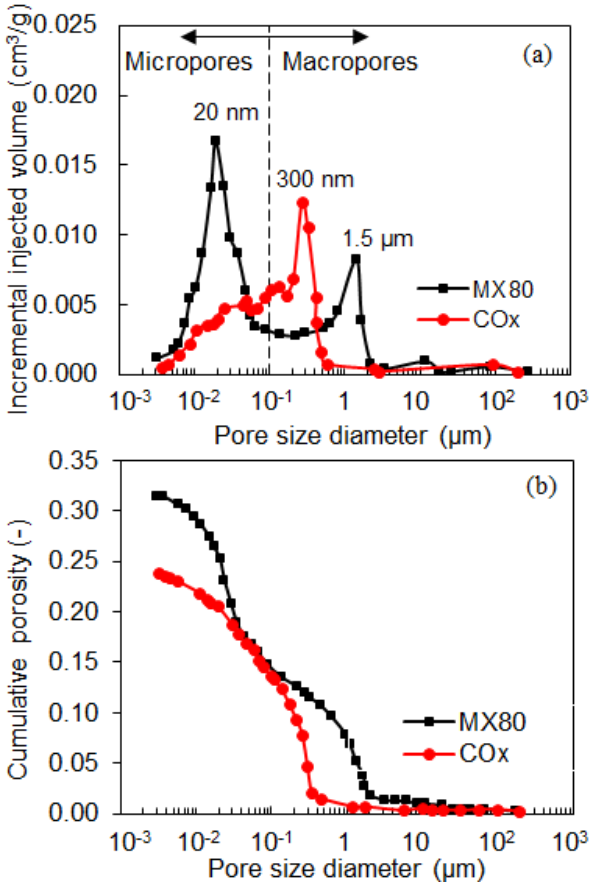

Figure 3 MIP tests on COx argillite MX80 bentonite compacted at dry density of 2.1 Mg/m^3: results in terms of (a) incremental injected volume of mercury and (b) cumulative porosity.

3.2 Test apparatus and experimental protocol

The swelling capacity of COx/MX80 mixtures was evalauted by performing swelling potential tests under constant vertical stress. An oedometric apparatus of high load capacity was used (Figure 4). The device constists of a metalic frame, devided in three parts; the cylindical cell containing the specimen (part 1 of

Figure 4), the piston located in the bottom of the cell, through which the vertical load is applied (part 2 of Figure 4) and the porcolation device in the upper part, responsible for the hydration of the sample (part 3 of Figure 4).

The cylindrical cell (d=40 mm) receives the soil specimen and a lid is screwed to ensure its confinement after the preparation. Porous disks are placed on both parallel sides of the specimen. A pressure sensor located on the cell's body allows the measurement of the radial stresses. On the top, one inlet allows the fluid infiltration and an outlet ensures the water saturation of the porous disk. The vertical load is applied through a hydraulic pump (maximum pressure capacity 60 MPa) by filling the space existing on the lower part of the piston with water (water chamber). O-rings installed on the piston are assuring the tighteness between the specimen and the water chamber. The unloading of the sample is carried out by carefully open the outlet valve on the bottom of water chamber, for water drainage. The stability of the applied vertical load during hydration is garanteed by an accumulator which regulates the applied stress. During the test, the sample's displacement is monitored by measuring the position of the piston by means of a displacement transducer.

The percolation device consists of a cylindrical container made of stainless steel, having at the upper part an inert fluid (helium) under a desired pressure and at the lower part the injection fluid. An oil interface of silicone limits the dissolution of the gas in the fluid. A sensor follows the injection pressure. The tank is connected with the cell through a valve. Its periodic weighing allows the measurement of the injected water injected and the permeability at saturation can be determined.

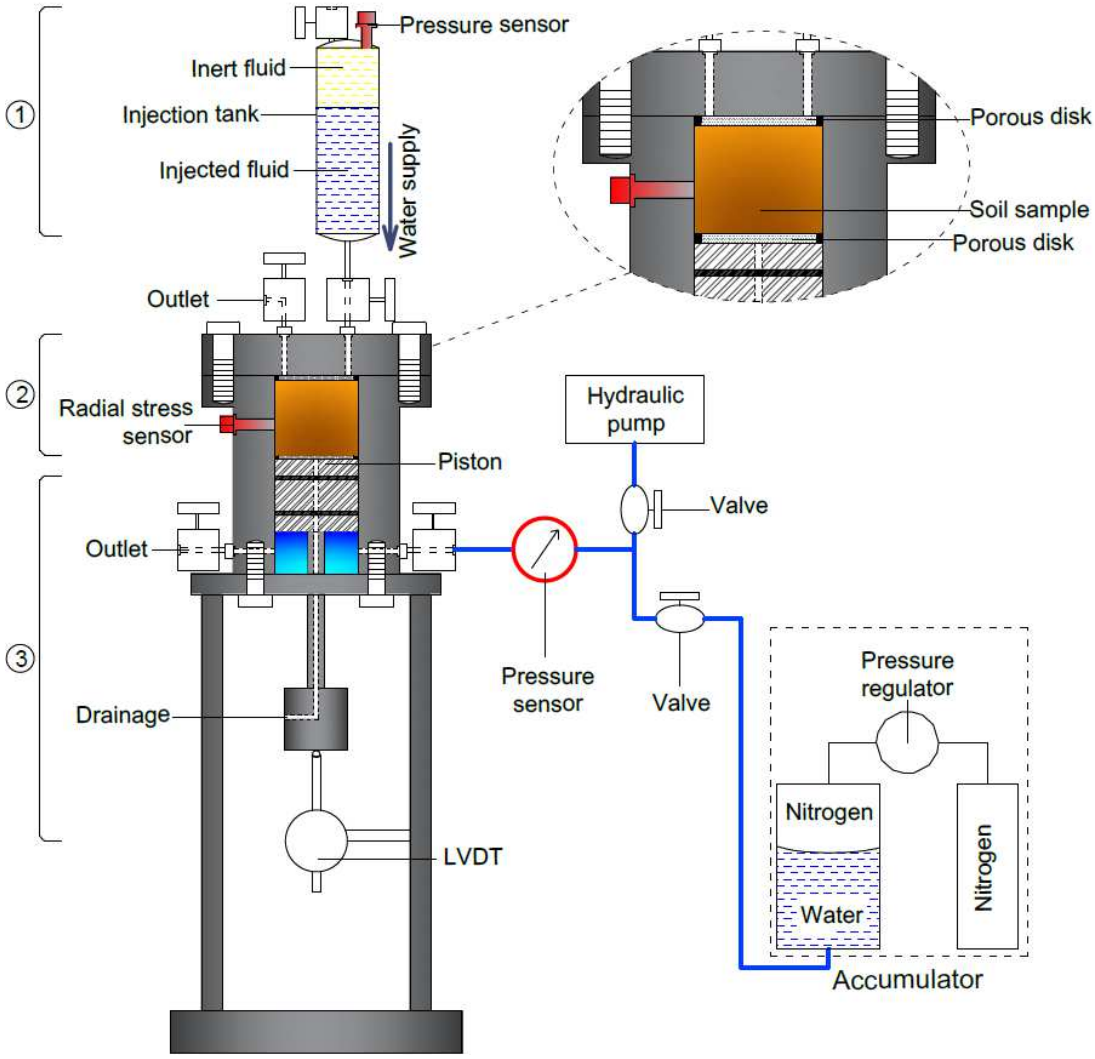

Figure 4 Schematic design of the high load capacity oedometric apparatus.

In the present study, COx/MX80 mixtures in various proportions of mass were tested (100/0, 95/5, 85/15, 70/30, 60/40, 50/50). The stress path followed upon the experiment is presented in Figure 5. Soil samples were compacted at initial water content, directly in the oedometric cell by applying a vertical stress $\sigma'_{i\ loading}$= 40 MPa (path AB of Figure 5) in order to achieve dry density of approximately 2.0 Mg/m^3 (simulating the manufacture conditions of the blocks). The specimens were then unloaded at the stress of $\sigma'_{i\ unloading}$= 4 MPa (path BC of Figure 5) and hydrated using demineralised water at constant injection pressure, while the applied stress was kept constant during the hydration process (path CD of Figure 5).

During the unloading path no significant change in the sample's dry density was observed. The axial strain of the sample was always monitored, corresponding the the material swelling potential. When the deformation was ceased, three permeability tests at saturated conditions were conducted (injection pressure of 1 MPa), by measuring the volume of the injected water.

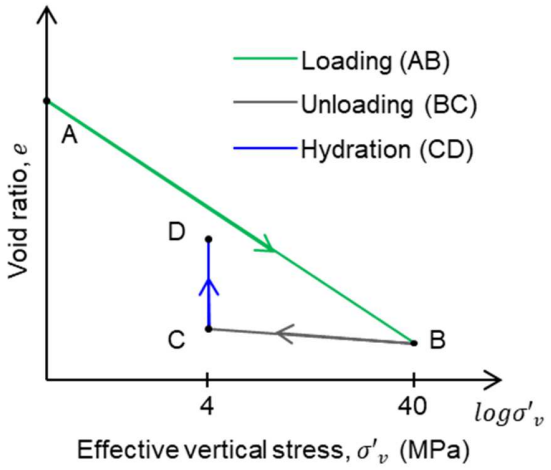

Figure 5 Generalized stress path followed on swelling under constant vertical stress tests.

4. Results and discussion

4.1 Fabric evolution at dry state

Figure 6 presents the results of the MIP tests on COx/MX80 mixtures in proportions of 60/40 and 30/70 respectively, compacted at dry density of 2.1 Mg/m^3. MX80 and COx samples with identical dry densities are also illustrated as reference.

For all samples containing MX80, the characteristic bimodal PSD is observed, contrary to the monomodal PSD of pure COx. A common peak at 20 nm is observed in the intra-aggregate domain and a pore population between 1.5-3 μm is identified in the intrer-aggregate domain, for the mixtures containing bentonite (Figure 6a). The micropores presence increases as MX80 is added in the mixture. At these highly compacted specimens (ρ_d = 2.1 Mg/m^3), micropore volume is more important than macropore

volume. The observation is in agreement with the compaction effect on macropores reported by previous studies (Lloret et al., 2003; Manca et al., 2015).

Even though the experimental method underestimates final porosity due to intrusion restrictions (Delage et al., 2006; Menaceur et al., 2016; Molinero Guerra et al., 2017; Molinero-Guerra et al., 2019), it is evident than adding bentonite increased progressively the mixture's final porosity (Figure 6b). However, a contradictory behaviour on the PSD is observed, with the bentonite addition to lead on slightly smaller macropores (1.5-3 μm) (Figure6a). It was expected that the MX80 addition would gradually increase macropores and thus the final porosity, as Figure 6b illustrated. Therefore, the variation of 1.5-3 μm is not considered notable and in fact it might be attributed to a not well-reprehensive sampling.

A comparison between the porosity of COx (n_{COx}) and the mixture containing 40% MX80 ($n_{40\%MX80}$) suggests that for lower bentonite contents no significant difference is observed (n_{COx}=24%, $n_{40\%MX80}$=27%) and therefore COx mainly governs the porosity.

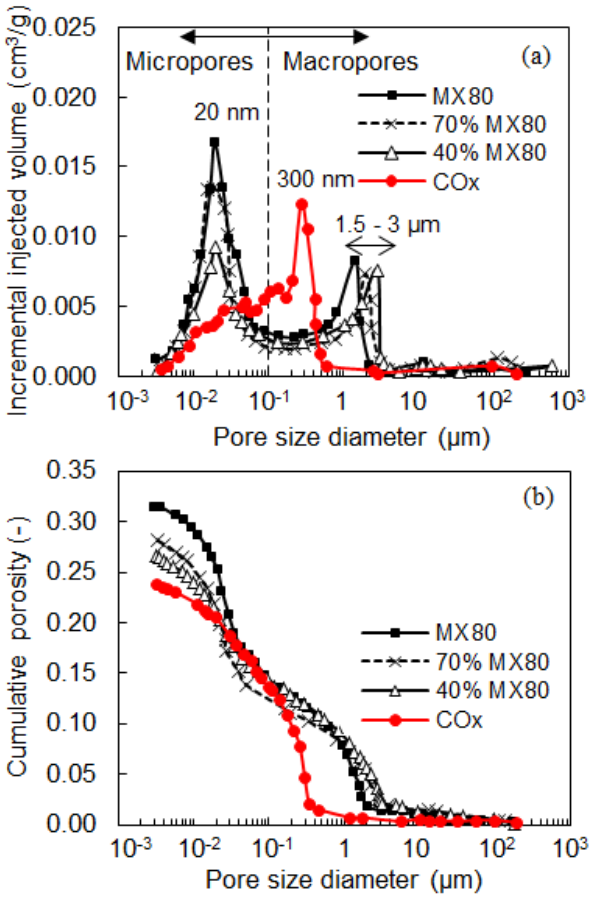

Figure 6 MIP tests on mixtures containing MX80 bentonite and COx argillite compacted at dry density of 2.1 Mg/m^3: results in terms of (a) incremental injected volume of mercury and (b) cumulative porosity.

4.2 Compressibility before hydration

Results for the loading/unloading path of pure COx and COx/MX80 mixtures are given at Figure 7, presented at the $e - log\sigma'_v$ plane. A linear relation is observed between the applied vertical stresses and the void ratio. A rather uniform behaviour on the loading/unloading path is observed for all tested mixtures. Details regarding the evolution of void ratio in the beginning of compaction e_0, the compression index C_C and swelling index C_S as function of the bentonite content are given on the first part of the supplementary material. It should be noted that the samples presented very low variation in their void ratio on the beginning of loading path (SD=0.03, CV=0.02). Additionally, compression index C_C and swelling index C_S were not strongly affected by the addition of MX80 bentonite in the mixture

(SD=0.01, CV=0.03 and SD=0.004, CV=0.20 respectively). In fact, the small-sized grains presented by both materials granulometry (D_{max}=300 µm) resulted into similar density upon the samples preparation (e_0). On the other hand, the high fine content of COx probably leads on a very similar behaviour upon compaction, for the tested bentonite contents. Figure 6b already showed that porosity does not significantly vary for this range of bentonite content. These results suggest that compressibility is mainly governed by the COx argillite presence. Since the coefficients did not depend on the bentonite content, average values could be chosen for the abovementioned parameters.

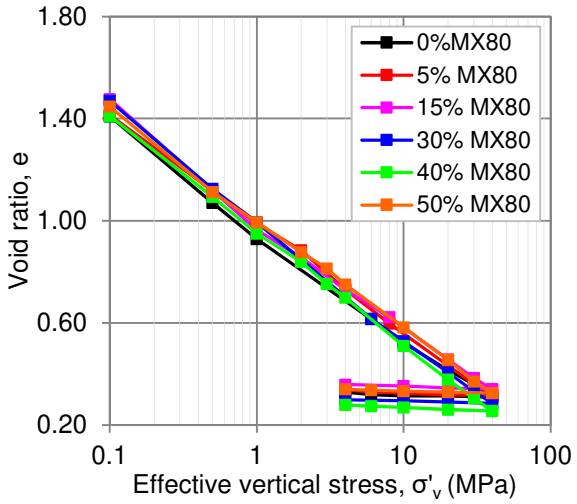

Figure 7 Compressibility curves for different COx/MX80 mixtures at initial non-hydrated conditions (loading up to 40 MPa, unloading at 4 MPa).

4.3 Water infiltration and hydro-mechanical behaviour

4.3.1 Swelling under 4 MPa

The materials capacity for void recovery was studied upon hydration under 4 MPa, on COx/MX80 mixtures previously compacted up to 40 MPa ($\rho_d = 2.0$ Mg/m^3). The swelling strain ε_S developed upon hydration was determined (in percentage) by the equation:

$$\varepsilon_S = \frac{\Delta H}{H_0} \ (\%) \qquad (1)$$

where ΔH is the displacement measured during the test in mm and H_0 the initial height of the specimen in mm before hydration. Figure 8 presents the final swelling strain measured for the COx/MX80 mixtures hydrated under 4 MPa as function of the bentonite content. Although COx presents swelling under these stress conditions, it is considerably low (ε_S =0.97%). The material's swelling performance is improved with MX80 addition. Swelling strain increases with bentonite content. A linear equation with high correlation is suggested to describe the relation between bentonite content and final swelling strain (%):

$$\varepsilon_S = 0.1681 B_c + 0.3368 \text{ with } R^2 = 0.991 \quad (2)$$

Detailed information of the obtained swelling potential results is presented on the second part of the supplementary material**.**

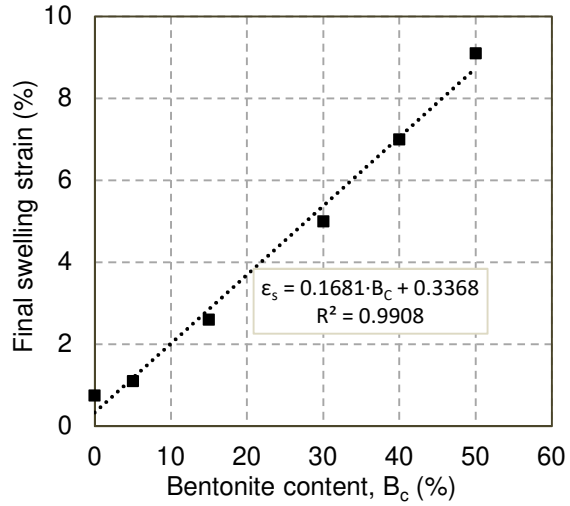

Figure 8 Final swelling strain under 4 MPa for different MX80 bentonite contents after compaction at 40 MPa (initial dry density of 2 Mg/m^3).

According to the experimental protocol followed by the present study, all specimens tested at swelling under constant vertical stress, present common stress history. The COx/MX80 samples were compacted at 40 MPa and unloaded at 4 MPa, resulting in overcosolidated samples (OCR=10). As Dang (2007) reported, samples compacted at a given loading stress, unloaded at a lower stress and hydrated while this stress is kept constant, form a curve which connects the saturation state with the loading conditions

(Figure 1). In that context, the saturation potential slope, λ_s can be determined by the conditions prevailing on the loading state and the experimentally measured saturated state.

Therefore, the experimental measuments of swelling under 4 MPa (saturation) and the material's loading state ($\sigma'_{i\,loading}$= 40 MPa) were used to determine the saturation potential slope λ_s of the tested COx/MX80 mixtures. The results are presented at Figure 9 as function of the bentonite content. The saturation potential slope λ_s clearly increases with MX80 addition. A nonlinear equation is used to describe this relation:

$$\lambda_s = 2 \cdot 10^{-5} \cdot {B_C}^2 - 1.2 \cdot 10^{-3} \cdot B_C + 0.0266, \quad \text{with } R^2=0.998 \qquad (3).$$

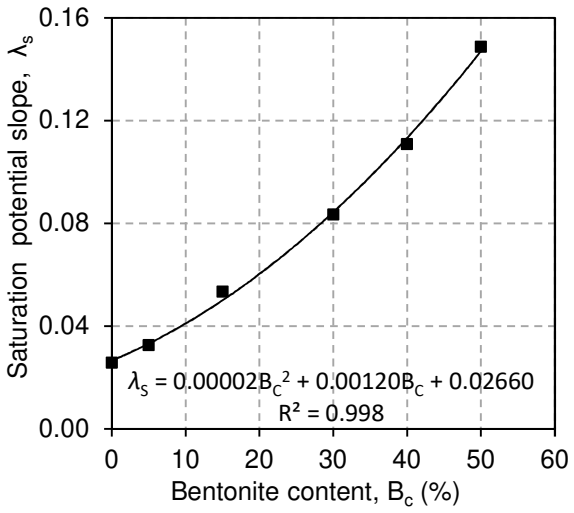

Figure 9 Measured saturation potential slope λ_s for different MX80 bentonite contents, compacted initially at 40MPa (initial dry density of 2 Mg/m^3) and unloaded at 4 MPa.

The evaluation of the proposed relation between saturation potential slope and bentonite content (eq. 3) was carried out by performing tests on additional COx/MX80 mixtures that followed similar stress paths. More precisely, two COx/MX80 mixtures were tested under different conditions:

- 10%MX80 compacted at 40 MPa, unloaded at 4 MPa (OCR=10) and hydrated under 4 MPa
- 70%MX80 compacted at 40 MPa, unloaded at 7 MPa (OCR=5.7) and hydrated under 7 MPa.

The selected mixtures corresponded to the MX80 range previously tested as well as higher values. The results of swelling under constant vertical stress were used to determine the saturation potential slope λ_s. The values of λ_s resulted from the measurements are compared with the values of saturation potential slope given by eq. 3 (Figure 10). Good correlation between the measured and the calculated values is observed for wide range of MX80 bentonite contents.

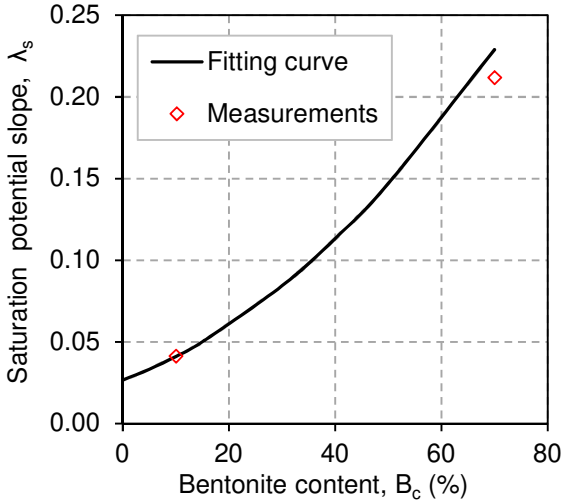

Figure 10 Evolution of saturation potential slope λ_S for different MX80 bentonite contents, calculated by the equation deduced by the experimental results. Two additional measures are used for comparison.

4.3.2 Saturated permeability

The groundwater infiltration will saturate the sealing material and thus its hydraulic performance at this permanent hydraulic state is studied**.** The saturated hydraulic conductivity K (in m/s) of the investigated COx/MX80 mixtures was determined by applying Darcy's law:

$$Q = K \cdot S \cdot \frac{\Delta h}{\Delta l} \quad (4)$$

where Q is the flow rate in m^3/s, S is the surface of the specimen in m^2, ΔH is the hydraulic head difference in m and Δl is the height of the specimen in m. Then, the intrinsic permeability, k (in m^2) was calculated as:

$$k = K \cdot \frac{\mu}{\rho \cdot g} \quad (5)$$

where K is the hydraulic conductivity in m/s, μ is the dynamic viscosity of the fluid in Pa.s (μ = 0.001 Pa.s for demineralized water), ρ is the fluid's density in kg/m^3 (ρ = 1000 kg/m^3 for demineralized water) and g is the gravity acceleration in m/s² (g = 9.81 m/s²). In total, three tests per sample are conducted and the final value is obtained as the average. Details are given on the third part of the provided supplementary material.

The intrinsic permeability is presented in Figure 11a as function of the bentonite content. For all the tested COx/MX80 mixtures, intrinsic permeability is ranging between 6×10^{-19} and 8×10^{-20} m². As it was expected, a clear influence of bentonite content is observed in the hydraulic performance of the material. The addition of MX80 in the mixture leads to higher swelling and therefore void decrease. Bentonite content and intrinsic permeability present a linear relation of high correlation:

$$k = 10^{-20} \cdot B_C + 5 \cdot 10^{-19} \text{ with } R^2 = 0.965 \quad (6)$$

where B_C is the bentonite content in %.

In order to evaluate further the effect of bentonite content on a mixture containing COx, permeability results from other studies using demineralized water are illustrated also in Figure 11b (Kohno et al., 2018; Komine, 2004b; Manca, 2015). Kunigel is also a sodium bentonite, with lower montmorillonite content (48%). The effect of bentonite on the mixture's permeability is clearly observed for every bentonite used. A less prominent variation is observed when COx is contained instead of sand. This might be attributed to the higher density of COx/MX80 mixtures (2.0 Mg/m^3) compared to the density values of the other studies, since density increase leads to lower hydraulic conductivity However, the influence of density seems to be less significant for bentonite contents higher than 40%.

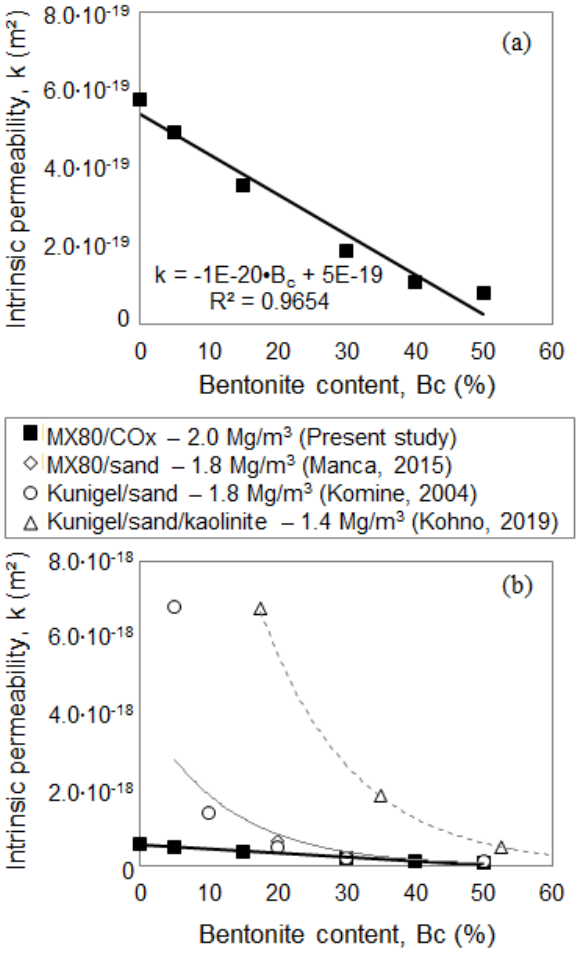

Figure 11 Evolution of saturated intrinsic permeability with bentonite content: (a) results of the present study for various COx/MX80 mixtures and (b) comparison between results of present and other studies on mixtures of MX80 and Kunigel bentonite with different soil materials.

4.4 Swelling estimation at higher compaction stresses

The design requirements indicated that at least 10% of swelling is requiered to fill the technological voids inside the repository. The swelling potential results under 4 MPa showed that this criterion was not fulfilled (maximum obtained $\varepsilon_S = 9\%$) for the tested COx/MX80 mixtures (Figure 9). Therefore, the concept of saturation potential slope (Figure 1) was adopted to identify the conditions (e.g. compaction state and/or COx/MX80 composition) where the target swelling potential could be achieved.

The variation of void ratio during swelling under constant vertical stress tests is illustrated in Figure 12, for different loading and unloading stresses. It has been designed considering that the saturation potential

slope (λ_s) depends only on the material and is not affected by the compaction stress ($\sigma'_{i\ loading}$) where the unloading path begins. Higher swelling is anticipated for samples subjected to higher compaction stress and unloaded at a common stress applied during hydration. The behavior is expected due to higher density resulted when higher compaction stress is applied (Villar and Lloret, 2008). In addition, for samples subjected to a common loading stress, higher swelling is expected when lower unloading stress is applied upon hydration (i.e. OCR increases) (Hoffmann et al., 2007; Komine et al., 2009; Villar et al., 2010; Yigzaw et al., 2016).

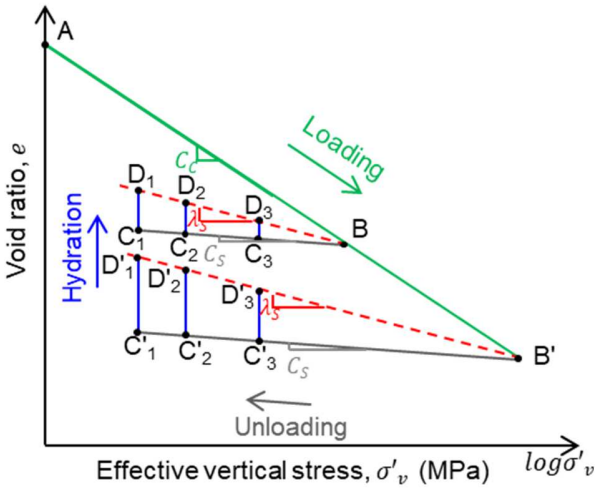

Figure 12 Variation of void ratio for over-consolidated COx/MX80 samples compacted at different stresses before unloading (σ'_B and $\sigma'_{B'}$) and saturated under various constant vertical stresses (σ'_{ci} and $\sigma'_{c'i}$).

Following these remarks, a method that estimates the swelling potential of various COx/MX80 mixtures is proposed for different compaction stresses ($\sigma'_{i\ loading}$) and unloading stresses during hydration ($\sigma'_{i\ unloading}$).

For the loading path, it is known that the void ratio at a given applied vertical stress $\sigma'_{i\ loading}$ is determined as:

$$e_{i\ loading} = e_0 - C_C . log\left(\frac{\sigma'_{i\ loading}}{\sigma'_0}\right) \quad (7)$$

where e_0 is the void ratio at the state prior to loading and C_C is the material's compression index. For the unloading path, the void ratio at a given $\sigma'_{i\ unloading}$ stress results from the equation:

$$e_{i\ unloading} = e_{loading} + C_S \cdot log\left(\frac{\sigma'_{loading}}{\sigma'_{i\ unloading}}\right) \quad (8).$$

where C_S is the material's swelling index. Void ratio at saturated state under a given constant vertical stress $\sigma_{i\ unloading}$ can be estimated from the saturation potential slope λ_s as:

$$e_{i\ saturated} = e_{i\ loading} + \lambda_s \cdot log\left(\frac{\sigma'_{i\ loading}}{\sigma'_{i\ unloading}}\right) \quad (9)$$

and the final swelling strain is calculated as follows:

$$\varepsilon_S(\%) = -\frac{e_{i\ unloading} - e_{i\ saturated}}{1 + e_{unloading}} \times 100 \quad (10).$$

In that framework, the swelling potential profile of various COx/MX80 mixtures was created for hydration under the investigated stress range of the design (1-7 MPa). Figure 13 illustrates the estimated final swelling for different COx/MX80 mixtures, compacted at different stresses and hydrated under 1 MPa, 4 MPa and 7 MPa; OCR index is also illustrated in a double x-axis. As it was expected, increase of compaction stress leads to specimens with higher density and therefore higher swelling is observed. The graphs show the combinations in terms of compaction stress and bentonite content that fulfil the design criteria in swelling capacity. In particular, swelling strain higher than 10% is obtained by COx/MX80 mixtures composed of at least 60% of MX80 bentonite, for the considered investigated stress range (1-7 MPa) and all applied maximum compaction stresses. Nevertheless, in case techno-economic purposes indicate lower bentonite contents, maximum compaction stresses larger than 40 MPa should be applied before the material's hydration. For instance, a mixture composed of 50% COx and 50% MX80 exhibits the target swelling strain under 7 MPa for compaction stress of 70 MPa. On the other hand, even if the highest maximum compaction stress ($\sigma'_{i\ loading}$= 80 MPa) is considered, COx/MX80 mixtures containing lower than 15% of MX80 do not present the desired swelling capacity. Depending on the design needs, an optimization of the material's characteristics can be obtained.

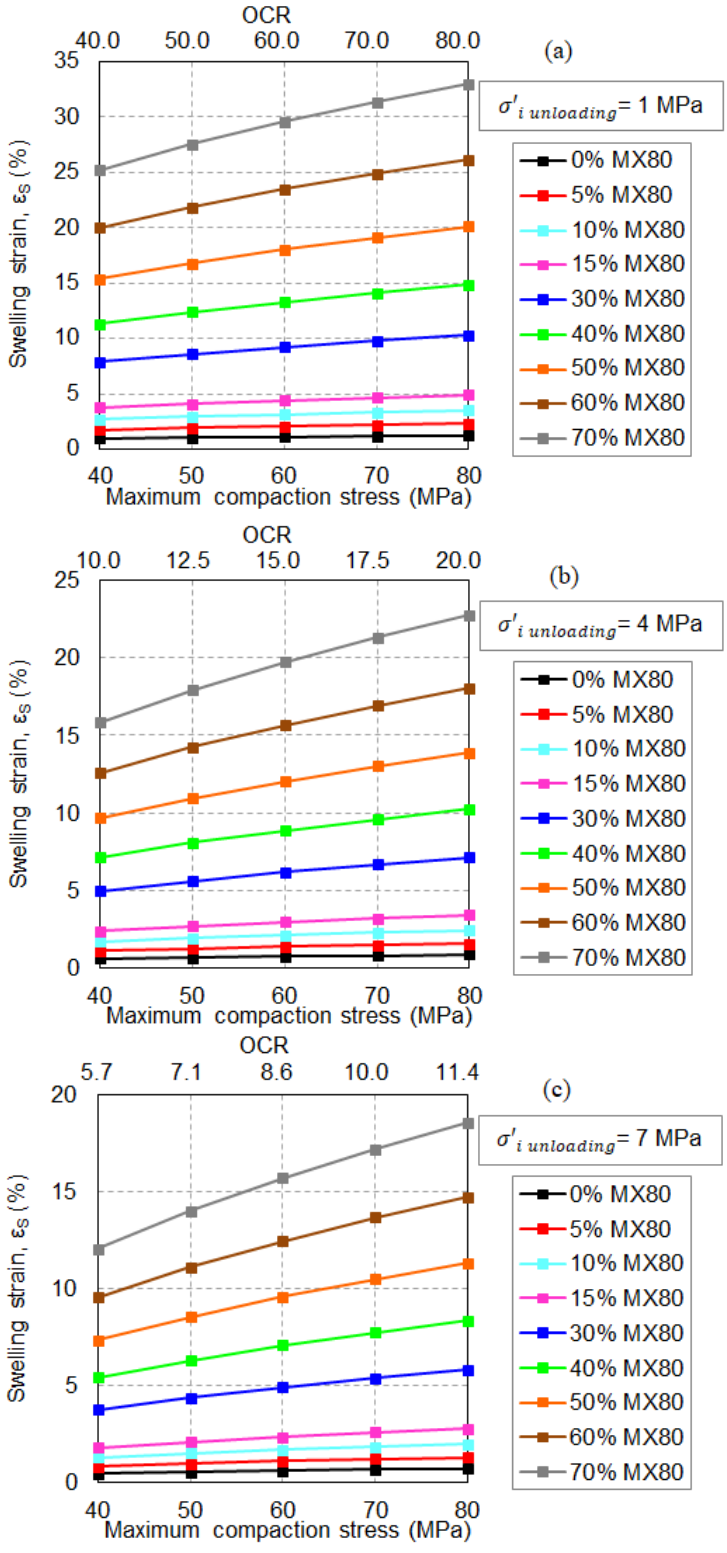

Figure 13 Swelling strain of saturated COx/MX80 mixtures as function of the maximum compaction stress, unloaded to (a) 1 MPa, (b) 4 MPa, (c) 7 MPa and as function of the resulting OCR.

5. Conclusions

The present experimental study focused on the hydro-mechanical behaviour of compacted materials as seals for the French radioactive waste disposal facilities. Mixtures composed of crushed COx and MX80 bentonite were compacted to exhibit dry density of 2.0 Mg/m^3, taking into consideration the implementation in prefabricated blocks. Both soil materials were sieved at D_{max}=300 μm.

Samples compacted at the initial water content showed a characteristic bimodal PSD when MX80 was contained, whereas pure COx exhibited monomodal PSD. The inter-aggregate pores of COx (300 nm) were smaller than the samples containing MX80 (1.5 - 3 μm). Micropores volume increased with bentonite addition. MX80 content gradually increased final porosity. However, no significant variation was observed for the lower MX80 contents.

A vertical stress of 40 MPa needs to be applied in order to achieve the materials desired dry density of 2.0 Mg/m^3. The rather uniform granulometry lead all mixtures to present similar void ratio since preparation. Compressibility was mainly governed by COx and was not affected by MX80 addition on the mixture.

The swelling under 4 MPa was measured for overconsolidated COx/MX80 samples with initial dry density ρ_d of 2.0 Mg/m^3 (OCR=10). The expected increase of swelling potential with bentonite addition was obtained. Contrary permeability on saturation decreased with the increase of bentonite percentage. The effect of bentonite on hydraulic performance was less significant for the highly compacted COx/MX80 mixtures in comparison to mixtures containing bentonite and sand/kaolinite.

The swelling potential results were combined with previous observations on overconsolidated specimens and the parameter of saturation potential slope λ_s was determined; it was highly affected by the MX80 content. The proposed relation of the two parameters was validated by data obtained from tests on additional COx/MX80 mixtures (OCR=5.7 and 10). The saturation potential slope was further adopted for the estimation of the swelling potential under 1 MPa, 4 MPa and 7 MPa for COx/MX80 mixtures loaded

1 at higher compaction stresses. As expected, swelling increases for higher compaction stress upon loading
2 or lower vertical stresses during hydration. From a practical point of view, the method identifies possible
3 combinations of compaction stress and bentonite content to fulfill the target design requirements for the
4 swelling potential.

Acknowledgements

The major part of laboratory work was performed at EGC (Euro-Géomat-Consulting) by Sy Quan Tu. Part of this work was financially supported by Andra (French Radioactive Waste Management Agency). The authors would like to thank Christophe Imbert for the fruitful discussions. The authors wish to thank also the editor and the reviewers for their helpful comments on the manuscript.

References

AFNOR, 1993. NF P 94-051. Soil : investigation and testing - Determination of Atterberg's limits - Liquid limit test using Casagrande apparatus - Plastic limit test on rolled thread. Association Française de Normalisation (AFNOR).

AFNOR, 1995. NF P94-052-1. Soil : investigation and testing - Atterberg limit determination - Part 1 : Liquid limit - Cone penetrometer method. Association Française de Normalisation (AFNOR).

AFNOR, 1998. NF P 94-068. Soils : Investigation and testing - Measuring of the methylene blue adsorption capacity of a rocky soil - Determination of the methylene blue of a soil by means of the stain test. Association Française de Normalisation (AFNOR).

AFNOR, 2002. XP P 84-703:2002-08. Bentonitic geosynthetics - Determination of the swelling capacity of clay in bentonitic geosynthetics. Association Française de Normalisation (AFNOR).

Andra, 2005a. Dossier 2005 Argile - Tome Architecture and management of a geological repository (No. Report No C.RP.ADP.04.0001).

Andra, 2005b. Dossier Synthesis - Evaluation of the feasibility of a geological repository in an argillaceous formation.

Andra, 2013. The Cigéo project - Meuse/Haute-Marne reversible geological disposal facility for radioactive waste.

Armand, G., Noiret, A., Zghondi, J., Seyedi, D.M., 2013. Short- and long-term behaviors of drifts in the Callovo-Oxfordian claystone at the Meuse/Haute-Marne Underground Research Laboratory. J. Rock Mech. Geotech. Eng. 5, 221–230. https://doi.org/10.1016/j.jrmge.2013.05.005

Armand, G., Leveau, F., Nussbaum, C., de La Vaissière, R., Noiret, A., Jaeggi, D., Landrein, P., Righini, C., 2014. Geometry and Properties of the Excavation-Induced Fractures at the Meuse/Haute-Marne URL Drifts. Rock Mech. Rock Eng. 47, 21–41. https://doi.org/10.1007/s00603-012-0339-6

Barast, G., Razakamanantsoa, A.-R., Djeran-Maigre, I., Nicholson, T., Williams, D., 2017. Swelling properties of natural and modified bentonites by rheological description. Appl. Clay Sci. 142, 60–68. https://doi.org/10.1016/j.clay.2016.01.008

Broc, D., Plas, F., Robinet, J.C., 1988. Mechanical properties of swelling Clays. MRS Online Proc. Libr. Arch. 127. https://doi.org/10.1557/PROC-127-669

Chandler, N.A., Cournut, A., Dixon, D., 2002. The five year report of the Tunnel Sealing Experiment: an international project of AECL, JNC, ANDRA and WIPP (No. AECL--12127). Atomic Energy of Canada Limited.

Chen, Y.-G., Zhu, C.-M., Ye, W.-M., Cui, Y.-J., Chen, B., 2016. Effects of solution concentration and vertical stress on the swelling behavior of compacted GMZ01 bentonite. Appl. Clay Sci. 124–125, 11–20. https://doi.org/10.1016/j.clay.2016.01.050

Chen, Y.-G., Dong, X.-X., Zhang, X.-D., Ye, W.-M., Cui, Y.-J., 2018. Combined thermal and saline effects on the swelling pressure of densely compacted GMZ bentonite. Appl. Clay Sci. 166, 318–326. https://doi.org/10.1016/j.clay.2018.10.001

Cuisinier, O., Deneele, D., Masrouri, F., Abdallah, A., Conil, N., 2014. Impact of high-pH fluid circulation on long term hydromechanical behaviour and microstructure of compacted clay from the laboratory of Meuse-Haute Marne (France). Appl. Clay Sci. 88–89, 1–9. https://doi.org/10.1016/j.clay.2013.12.008

Dang, K.D., 2007. Contribution à l'étude du comportement thermo-hydro-mécanique des matériaux argileux (bentonite MX80 et argilite du Callovo-oxfordienne) (PhD Thesis). Rennes, INSA.

Davies, C.W., Davie, C.T., Charles, E.A., White, M., 2017. Physicochemical and geotechnical alterations to MX-80 bentonite at the waste canister interface in an engineered barrier system. Geosciences 7. https://doi.org/10.3390/geosciences7030069

Delage, P., Marcial, D., Cui, Y.J., Ruiz, X., 2006. Ageing effects in a compacted bentonite: a microstructure approach. Géotechnique 56, 291–304. https://doi.org/10.1680/geot.2006.56.5.291

Di Maio, C., Santoli, L., Schiavone, P., 2004. Volume change behaviour of clays: the influence of mineral composition, pore fluid composition and stress state. Mech. Mater., Coupled Chemo-Mechanical Phenomena 36, 435–451. https://doi.org/10.1016/S0167-6636(03)00070-X

Feng, M., Gan, J.K.M., Fredlund, D.G., 1998. A laboratory study of swelling pressure using various test methods, in: Proceedings of the Second International Conference on Unsaturated Soils (UNSAT-98), Beijing. pp. 350–355.

Foin, R., Bosgiraud, J.M., Armand, G., Noiret, A., 2015. Technical feasibility of the Cigéo Project seals. Proc. LUCOEX Conf. Workshop June 2-4 2015 Oskarshamn Swed.

Gens, A., Alonso, E.E., 1992. A framework for the behaviour of unsaturated expansive clays. Can. Geotech. J. 29, 1013–1032.

Hoffmann, C., Alonso, E.E., Romero, E., 2007. Hydro-mechanical behaviour of bentonite pellet mixtures. Phys. Chem. Earth Parts ABC, Clay in natural and engineered barriers for radioactive waste confinement - Part 2 32, 832–849. https://doi.org/10.1016/j.pce.2006.04.037

Imbert, C., Villar, M.V., 2006. Hydro-mechanical response of a bentonite pellets/powder mixture upon infiltration. Appl. Clay Sci. 32, 197–209. https://doi.org/10.1016/j.clay.2006.01.005

Karnland, O., Olsson, S., Nilsson, U., Sellin, P., 2007. Experimentally determined swelling pressures and geochemical interactions of compacted Wyoming bentonite with highly alkaline solutions. Phys. Chem. Earth Parts ABC, Clay in natural and engineered barriers for radioactive waste confinement - Part 1 32, 275–286. https://doi.org/10.1016/j.pce.2006.01.012

Karnland, O., Nilsson, U., Weber, H., Wersin, P., 2008. Sealing ability of Wyoming bentonite pellets foreseen as buffer material – Laboratory results. Phys. Chem. Earth Parts ABC, Clays in Natural & Engineered Barriers for Radioactive Waste Confinement 33, S472–S475. https://doi.org/10.1016/j.pce.2008.10.024

Kohno, M., Nara, Y., Kato, M., Nishimura, T., 2018. Effects of clay-mineral type and content on the hydraulic conductivity of bentonite–sand mixtures made of Kunigel bentonite from Japan. Clay Miner. 53, 721–732. https://doi.org/10.1180/clm.2018.52

Komine, H., 2004a. Simplified evaluation for swelling characteristics of bentonites. Eng. Geol. 71, 265–279. https://doi.org/10.1016/S0013-7952(03)00140-6

Komine, H., 2004b. Simplified evaluation on hydraulic conductivities of sand–bentonite mixture backfill. Appl. Clay Sci. 26, 13–19.

Komine, H., Yasuhara, K., Murakami, S., 2009. Swelling characteristics of bentonites in artificial seawater. Can. Geotech. J. 46, 177–189. https://doi.org/10.1139/T08-120

Lee, J.O., Lim, J.G., Kang, I.M., Kwon, S., 2012. Swelling pressures of compacted Ca-bentonite. Eng. Geol. 129–130, 20–26. https://doi.org/10.1016/j.enggeo.2012.01.005

Lloret, A., Villar, M.V., Sánchez, M., Gens, A., Pintado, X., Alonso, E.E., 2003a. Mechanical behaviour of heavily compacted bentonite under high suction changes. Géotechnique 53, 27–40. https://doi.org/10.1680/geot.2003.53.1.27

Manca, D., 2015. Hydro-chemo-mechanical characterisation of sand/bentonite mixtures (PhD Thesis). École Polytechnique Fédérale de Lausanne.
Manca, D., Ferrari, A., Laloui, L., 2015. Fabric evolution and the related swelling behaviour of a sand/bentonite mixture upon hydro-chemo-mechanical loadings. Géotechnique 66, 41–57. https://doi.org/10.1680/jgeot.15.P.073
Menaceur, H., Delage, P., Tang, A.M., Talandier, J., 2016. The Status of Water in Swelling Shales: An Insight from the Water Retention Properties of the Callovo-Oxfordian Claystone. Rock Mech. Rock Eng. 49, 4571–4586. https://doi.org/10.1007/s00603-016-1065-2
Mishra, A.K., Ohtsubo, M., Li, L.Y., Higashi, T., Park, J., 2009. Effect of salt of various concentrations on liquid limit, and hydraulic conductivity of different soil-bentonite mixtures. Environ. Geol. 57, 1145–1153. https://doi.org/10.1007/s00254-008-1411-0
Mitchell, J.K., Soga, K., 2005. Fundamentals of soil behavior. John Wiley & Sons New York.
Molinero Guerra, A., Mokni, N., Delage, P., Cui, Y.-J., Tang, A.M., Aimedieu, P., Bernier, F., Bornert, M., 2017. In-depth characterisation of a mixture composed of powder/pellets MX80 bentonite. Appl. Clay Sci. 135, 538–546. https://doi.org/10.1016/j.clay.2016.10.030
Molinero Guerra, A., Aimedieu, P., Bornert, M., Cui, Y.-J., Tang, A.M., Sun, Z., Mokni, N., Delage, P., Bernier, F., 2018. Analysis of the structural changes of a pellet/powder bentonite mixture upon wetting by X-ray computed microtomography. Appl. Clay Sci. 165, 164–169. https://doi.org/10.1016/j.clay.2018.07.043
Molinero-Guerra, A., Delage, P., Cui, Y.-J., Mokni, N., Tang, A.M., Aimedieu, P., Bernier, F., Bornert, M., 2019. Water-retention properties and microstructure changes of a bentonite pellet upon wetting/drying; application to radioactive waste disposal. Géotechnique 70, 199–209. https://doi.org/10.1680/jgeot.17.P.291
Pusch, R., 1982. Mineral–water interactions and their influence on the physical behavior of highly compacted Na bentonite. Can. Geotech. J. 19, 381–387. https://doi.org/10.1139/t82-041
Rao, S.M., 2006. Identification and classification of expansive soils. Taylor and Francis, London.
Robinet, J.C., Gatabin, C., Imbert, C., Michau, N., 2003. Study of the effectes of an alkaline plume on the hydraulic and hydro-mechanical properties of the bentonite MX80- Final Report ANDRA C.RP.0EUG.02.009.
Romero, E., 2013. A microstructural insight into compacted clayey soils and their hydraulic properties. Eng. Geol., Special Issue: Research and Applications in Unsaturated Soil Mechanics 165, 3–19. https://doi.org/10.1016/j.enggeo.2013.05.024
Seiphoori, A., Ferrari, A., Laloui, L., 2014. Water retention behaviour and microstructural evolution of MX-80 bentonite during wetting and drying cycles. Géotechnique 64, 721–734. https://doi.org/10.1680/geot.14.P.017
Sridharan, A., Rao, A.S., Sivapullaiah, P.V., 1986. Swelling Pressure of Clays. Geotech. Test. J. 9, 24–33. https://doi.org/10.1520/GTJ10608J
Tang, C.S., Tang, A.M., Cui, Y.J., Delage, P., Schroeder, C., De Laure, E., 2011a. Investigating the swelling pressure of compacted crushed-Callovo-Oxfordian claystone. Phys. Chem. Earth Parts ABC, Clays in Natural & Engineered Barriers for Radioactive Waste Confinement 36, 1857–1866. https://doi.org/10.1016/j.pce.2011.10.001
Tang, C.S., Tang, A.M., Cui, Y.J., Delage, P., Schroeder, C., Shi, B., 2011b. A study of the hydro-mechanical behaviour of compacted crushed argillite. Eng. Geol. 118, 93–103. https://doi.org/10.1016/j.enggeo.2011.01.004
Villar, M.V., Lloret, A., 2008. Influence of dry density and water content on the swelling of a compacted bentonite. Appl. Clay Sci. 39, 38–49. https://doi.org/10.1016/j.clay.2007.04.007
Villar, M.V., Gómez-Espina, R., Lloret, A., 2010. Experimental investigation into temperature effect on hydro-mechanical behaviours of bentonite. J. Rock Mech. Geotech. Eng. 2, 71–78. https://doi.org/10.3724/SP.J.1235.2010.00071
Villar, M.V., Gómez-Espina, R., Gutiérrez-Nebot, L., 2012. Basal spacings of smectite in compacted bentonite. Appl. Clay Sci. 65–66, 95–105. https://doi.org/10.1016/j.clay.2012.05.010

Wang, Q., Tang, A.M., Cui, Y.-J., Delage, P., Gatmiri, B., 2012. Experimental study on the swelling behaviour of bentonite/claystone mixture. Eng. Geol. 124, 59–66. https://doi.org/10.1016/j.enggeo.2011.10.003

Ye, W.M., Zheng, Z.J., Chen, B., Chen, Y.G., Cui, Y.J., Wang, J., 2014. Effects of pH and temperature on the swelling pressure and hydraulic conductivity of compacted GMZ01 bentonite. Appl. Clay Sci. 101, 192–198. https://doi.org/10.1016/j.clay.2014.08.002

Yigzaw, Z.G., Cuisinier, O., Massat, L., Masrouri, F., 2016. Role of different suction components on swelling behavior of compacted bentonites. Appl. Clay Sci. 120, 81–90. https://doi.org/10.1016/j.clay.2015.11.022

Yven, B., Sammartino, S., Geraud, Y., Homand, F., Villieras, F., 2007. Mineralogy, texture and porosity of Callovo-Oxfordian argillites of the Meuse/Haute-Marne region (eastern Paris Basin). Mém. Société Géologique Fr. 178, 73–90.

Zhang, C.-L., Kröhn, K.-P., 2019. Sealing behaviour of crushed claystone–bentonite mixtures. Geomech. Energy Environ., Geomechanics for nuclear waste storage 17, 90–105. https://doi.org/10.1016/j.gete.2018.09.004